

Novel design measures for optimizing the yearlong performance of a concentrating solar thermal power plant using thermal storage and a dry-cooled supercritical CO₂ power block



M. Monjurul Ehsan*, Zhiqiang Guan, Hal Gurgenci, Alexander Klimenko

Renewable Energy Conversion Centre of Excellence, School of Mechanical and Mining Engineering, The University of Queensland, Brisbane, QLD 4072, Australia

ARTICLE INFO

Keywords:

Dry cooling
Concentrated solar power
Supercritical CO₂
Thermal storage
Cooling tower
Molten salt

ABSTRACT

Owing to water deficit and environmental concerns, the compatibility of dry cooling technology with supercritical CO₂ (sCO₂) power cycle in concentrated solar power (CSP) offers superior performance even at extreme climate temperatures. The CSP plant performance is expressively dominant by the erratic attributes of solar insolation and varying ambient temperature. In the present work, the dynamic attributes of the dry cooled sCO₂ recompression cycle coupled with the central receiver is presented in terms of net power generation at different climate conditions. The supplementary bypass arrangement prior to the dry cooling tower ensures the system operating at the design point compressor inlet temperature in the occasion of low ambient temperatures. Solar tower plant with molten salt thermal energy storage is used to supply dispatchable electricity during nighttime. Based on the annual climate temperature profile, two sets of ambient air temperatures are selected for the cooling system design. This requires the rectification of two sets of design point main compressor inlet temperature/tower exit temperature at optimum turbine exhaust pressure in advance of the integration and design of the dry cooling tower. The key parameters of the solar system (cold tank temperature and molten salt split ratio) and power block (MCIT, pressure ratio, cycle mass, and bypass fraction) are optimized to maximize the power generation at any circumstances. The required height of the tower is 59 m and 67 m at two design points. The average net power using the minimum climate temperature is 23.71 MW and 24.09 MW respectively, whereas using the maximum climate temperature the values are 23.06 MW and 23.45 MW. The dynamic response from the system when the thermal energy storage operates during nighttime using additional bypass is demonstrated under the fluctuation of air temperature. The year-round plant performance as well as the dynamic response from the cooling tower of both cases are assessed with the historical air temperature data.

1. Introduction

The government agencies and policymakers around the world have been emphasizing the execution of new technologies to subside the energy crisis with clean and renewable energy. Substantial attention has been devoted to the research and development of the conversion of solar thermal energy to electricity in order to reduce fossil fuel energy consumption [1]. In concentrated solar power application, dry cooling is receiving remarkable attention as a suitable substitute for wet cooling systems due to the inaccessibility of ample water supply [2,3]. The sCO₂ with its affirmative thermodynamic properties (lower critical parameters, higher specific heat and density in the vicinity of critical condition) provide superior thermal performance compared to the traditional steam cycles [4,5]. The superior chemical properties of sCO₂ (global warming potential of 1, zero ozone depletion potential, non-

combustible, non-corrosive and non-hazardous) provide complete environmental protection and safe operation [6,7].

1.1. The superiority of sCO₂ cycles

Persichilli et al. [5] reported the potentials of supercritical CO₂ power cycles over Rankine cycles by highlighting its compactness, lower cost, and higher cycle efficiency. Besarati and Goswami [8] assessed the potential of different sCO₂ power cycles among which partial cooling and intercooling configuration showed promising performance. Dyreby et al. [9] performed the optimization of a simple and recompression sCO₂ cycles. They studied the relationship between the recuperator size and the cycle lowest temperature in order to maximize the cycle efficiency. Wright et al. [10] reported on *trans*-critical CO₂ cycle tests in Sandia national laboratory that observe the improvement

* Corresponding author.

E-mail address: m.ehsan@uqconnect.edu.au (M. Monjurul Ehsan).

<https://doi.org/10.1016/j.enconman.2020.112980>

Received 10 February 2020; Received in revised form 10 May 2020; Accepted 14 May 2020

Available online 22 May 2020

0196-8904/ © 2020 Elsevier Ltd. All rights reserved.

Nomenclature

A	Area, m ²
C _p	Specific heat at constant Pressure, J/kgK
C _{Dts}	Drag coefficient
d	Diameter, m
f	Friction factor
F _T	Correction factor
Fr _D	Froude number
F _{Dts}	Drag force, N
H	Heat transfer coefficient, W/m ² K
H	Height, m
K	Thermal conductivity, W/mK
K	Loss coefficient
l _{ts}	Length of tower support, m
L _t	Length of tube, m
M _{cf}	sCO ₂ mass flow, kg/s
M _s	Molten salt mass flow, kg/s
M _a	Air mass flow, kg/s
M _t	Solar tank capacity, kg
N	Number of segments
N	Number of heliostats
n _{ts}	Number of tower supports
n _r	Number of tube rows
n _b	Number of tubes per bundle
n _{tr}	Effective number of tubes per row
P _f	Fin pitch, m
P _t	Transversal tube pitch, m
P _l	Longitudinal tube pitch, m
P _d	Diagonal tube Pitch, m
Q	Heat transfer rate, W
U	Overall heat transfer coefficient, W/m ² K
Q	Heat flux, W/m ²
T	Temperature, K
t _f	Fin thickness (mean), m
t _{ft}	Fin tip thickness, m
t _{fr}	Fin root thickness, m
η	Plant efficiency
η _{th}	Cycle efficiency

Subscript

a	air side
---	----------

B	bulk, Heat exchanger bundles
ct	cooling tower
ctc	cooling tower contraction
cte	cooling tower expansion
cv	control volume
f	fin
frT	total frontal
he	heat exchanger
pc	pseudocritical
r	root
s	supercritical; support
t	tube side
to	tower outlet
ts	tower support

Dimensionless parameter

Nu	Nusselt number
Pr	Prandtl number
Re	Reynolds number
Ry	Characteristics Reynolds number

Abbreviations

ACHE	air-cooled heat exchanger
CSP	concentrated solar power
DP	design point
DNI	direct normal irradiance
HTR	high-temperature recuperator
LTR	low-temperature recuperator
MCIT	main compressor inlet temperature
MDK	model development kit
MDL	model development language
MSHE	molten salt heat exchanger
NDDCT	natural draft dry cooling tower
sCO ₂	supercritical CO ₂
TES	thermal energy storage
TIT	turbine inlet temperature

of cycle performance over the Rankine cycle. Incorporating the multiple reheat stage between the turbines further increased the efficiency by 4–5%. Marchionni et al. [11] conducted the thermo-economic investigation of four different layouts of sCO₂ bottoming cycle cascaded with a steam Rankine cycle to utilize the waste heat. Cao et al. [12] also conducted the combined supercritical and *trans*-critical CO₂ cycle study to observe the performance improvement of 17% compared to a simple regenerative cycle. Kim et al. [13] enhanced the sCO₂ recompression cycle performance based on the recuperator effectiveness and pinch point temperature restraint in the recuperator. The split ratio and pressure ratio were also optimized.

1.2. CSP plants integrated with sCO₂ power cycles

Zhu and He [14] studied the impact of turbine inlet temperature on four different layouts of power cycles coupled with a central receiver where the sCO₂ was directly heated in the receiver and was employed as for both heat transfer and working fluid. Wang et al. [15,16] comprehensively investigated the system performance of several solar-assisted sCO₂ power cycles with a molten salt technology thermal energy

storage system. Padilla et al. [17] reported a comprehensive exergetic analysis with various solar-assisted sCO₂ closed-loop Brayton cycle configurations with recuperation and recompression. They observed the recompression cycle can provide the best exergetic performance and highest thermal efficiency of 55.2% at 850 °C. sCO₂ recompression cycle they proposed could be a viable candidate for central solar receiver systems. Singh et al. [18] reported the influence of ambient air temperature and solar energy input on the performance of direct heated sCO₂ Brayton cycles during winter and summer by conducting dynamic simulations. Osorio et al. [19] reported the transient analysis of the recompression cycle for solar energy application under different seasonal variations. The influence of the mass flow rate, the operating pressure, the effective recuperator area, the number of stages during compression and expansion were analyzed based on the overall plant efficiency.

1.3. Dry cooling compatibility with sCO₂ cycles

Dunham and Iverson [20] compared the cycle efficiency of various dry-cooled power cycles for solar application. Singh et al. [21]

proposed an extremum seeking controller to maximize the power generation of a solar-assisted sCO_2 recuperated cycle at variant solar insolation and environmental temperature. Zeyghami and Khalili [22] reported an efficiency enhancement of 5–7% with the implementation of a daytime radiative cooling in addition to the dry cooler in a sCO_2 recuperated and recompression cycle. The required radiative cooler area to achieve this improvement was reported. The influence of pressure drop and reheat stage on the cycle efficiency, solar field and receiver performance performed for a dry-cooled sCO_2 CSP plant [23]. At higher ambient temperature, the performance of a dry-cooled CSP plant can be compensated by increasing the main compressor inlet pressure [24]. Recently, Luu et al. [25] studied the advanced control strategies of startup operation comprised of four phases in a recompression sCO_2 cycle using dry cooling.

In our past research, a detailed dry cooling tower model was developed with MATLAB code to assess the suitability of the cooling circuit (direct and indirect) in a sCO_2 power cycle [26,27]. The influence of cooling system design parameters on the recompression cycle performed under variant working conditions [28]. A comprehensive economic analysis performed for the natural draft dry cooling tower (NDDCT) and various geometric variables of the cooling system were optimized [29]. The valuation of the power cycle coupled with NDDCT carried out by evaluating the cycle efficiency, exergy efficiency, and cooling tower effectiveness.

2. Research question and scope

In a dry cooled CSP plant, the power fluctuation occurs not only due to the fluctuation of solar irradiance throughout the year but also with the variation of ambient conditions. The variation of ambient temperature changes the NDDCT exit temperature which subsequently alters the system performance from the design condition. Hence, plant performance is vastly influenced by the intermittent nature of solar insolation and air temperature. The previous research from the literature emphasized the dynamic behavior of the CSP plant with the alteration of solar energy and the cooling system operated under the prescribed condition with the assumption of fixed compressor inlet temperature. This research question is investigated by examining the dynamic performance of a dry cooled CSP plant coupled with the sCO_2 recompression cycle. The emphasis is paid on the cooling tower off-design performance at variant ambient conditions and the overall plant performance at different seasonal conditions. The molten salt two-tank

thermal energy storage (TES) is equipped with the central receiver to provide uninterrupted power production during nighttime operation. The scope of our work is demonstrated below.

- (i) The influence of the main compressor inlet temperature (MCIT) on the design of a CSP plant is performed in order to rectify an optimal MCIT based on which the dry cooling tower is designed.
- (ii) Based on the year-round ambient temperature profile, two design point MCITs at different compressor inlet pressure are identified to design the cooling system for two scenarios. The heliostat field design, the temperature of the two tanks, the thermal mass of TES are evaluated based on optimal MCIT condition.
- (iii) The inclusion of NDDCT flow by-pass arrangement helps to operate the plant at design point MCIT condition in the occasion of lower ambient temperature. The year-round cooling tower off-design performance and overall system dynamic attributes are assessed and compared for two scenarios of design point ambient temperatures.
- (iv) The contribution of TES during nighttime and the corresponding dynamism in power generation is demonstrated for different seasonal time (summer, winter, autumn, and spring).

3. Modelling of Dry-cooled sCO_2 CSP plant

The Recompression cycle layout is a potential candidate for ****integration in future CSP plants due to its less complexities in the power block and the elimination of pinch point development in the recuperators [30,31]. The CSP is equipped with TES for nighttime operation as demonstrated in Fig. 1. The heat transfer fluid used in the CSP is nitrate salt ($NaNO_3$ -60% wt, KNO_3 -40% wt). The molten salt split ratio, SR_s accounts for salt stored in the TES following its charging hour. The remaining salt flows into the MSHE to provide the required thermal energy in the power block. The solar salt exchanges its thermal energy in the MSHE with the high-pressure sCO_2 stream from the HTR outlet (process 3–4). Hence, the cycle fluid is indirectly heated in the MSHE to deliver the cycle maximum temperature (process 4–5). The hot turbine exhaust still offers further heat recovery with the recuperators (process 6–7 and 7–8). At state point 8, the outlet of low-pressure LTR stream is by-passed with a flow splitter before entering the cooling system. This is known as cycle fluid split ratio, SR_c an important parameter determined by the pinch point constraint in the LTR side. The air-cooled heat exchanger (ACHE) unit inside the NDDCT cools the

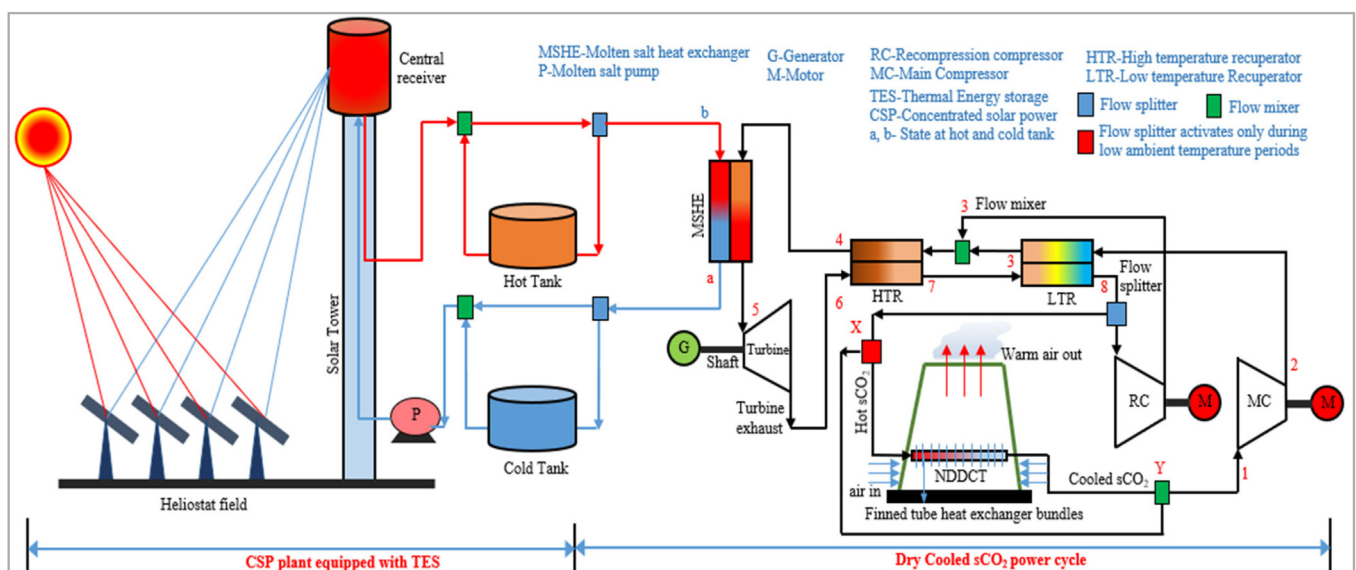


Fig. 1. Schematic of a dry cooled sCO_2 CSP plant with TES.

sCO₂ to the desired cycle minimum temperature (process 8–1) before it is compressed by the MC to the cycle highest pressure (process 1–2). The high-pressure stream is preheated in the recuperators (process 2–3 and 3–4) before it is being heated in MSHE.

An additional flow splitter prior to the NDDCT (state X) is used on the occasion of low climate temperature to prevent cycle overcooling. The heat rejection in the cooling tower can be reduced with this flow splitter. A portion of the sCO₂ stream is extracted and then mixed (state Y) with the outlet of the NDDCT stream to provide the required MCIT. The mechanism of this additional flow splitter during low air temperature period is described in the result section. The location of the CSP plant in the present work is Alice Spring, NT, Australia (latitude-23.8°S, longitude-133.89°E, elevation-546 m, and station number-15590). Table 1 shows the model equations of the proposed CSP plant integrated with TES.

3.1. Air temperature selection

The year-round air temperature variation and the DNI fluctuation in Alice spring are shown in Fig. 2(a) and 2(c). The intermittent nature of DNI severely impacts the plant performance during daytime as well as low DNI seasons. The heat input to the power cycle from the CSP plant is highly influenced by the DNI variation whereas, the power cycle minimum temperature (MCIT) is dominated by the climate temperature. During nighttime when no solar energy is available, the TES can supply constant thermal energy to the power block for a certain period of time. However, the plant performance still fluctuates since the air temperature varies during nighttime. In a CSP location, the choice of this air temperature is crucial to model the dry cooling tower. The frequency histogram of daily mean temperature is shown in Fig. 2(b).

Table 1
Modelling equations of the CSP plant and power block.

Heliostat Field	Parameter/Component	Equation
	Solar declination angle [32], δ	$\delta = \frac{23.45\pi}{180} \sin(2\pi \frac{284 + n_d}{365})$ Here, n_d is the day of year.
	Solar altitude [32], α_S	$\alpha_S = \sin^{-1}(\cos \Phi \cos \delta \cos \omega_S + \sin \Phi \sin \delta)$ Here, Φ is the latitude angle and ω_S is the hour angle.
	Solar azimuth angle [32], γ_S	$\gamma_S = \sin \omega_S \left[\cos^{-1} \frac{\sin \Phi \sin \delta - \sin \delta}{\cos \alpha_S \cos \Phi} \right]$
	Efficiency of heliostat field [32], η_{opt}	$\eta_{opt}(x, y, t) = \rho \cos \omega(x, y, t) f_{at}(x, y) f_{sb}(x, y, t) f_{lic}(x, y, t)$ Here, ω is angle between incident ray and the normal to the heliostat surface, f_{at} is the atmospheric attenuation efficiency, f_{sb} is blocking factor, f_{lic} is the intercept factor by the central receiver, and x, y, t represents co-ordinates and time.
Central receiver	Heat loss due to solar radiation [33], Q_{rad}	$Q_{rad} = F_{view} A \sigma \epsilon T_R^4$ Here, F_{view} is the shape factor due to radiation, A is the central receiver radiative area, ϵ is the emissivity of the receiver, σ is the Stefan Boltzmann constant, and T_R is the temperature of the central receiver.
	Convective heat transfer [33], Q_{conv}	$Q_{conv} = A h_{conv} f_{conv} (T_R - T_{amb})$ Here, T_{amb} is the atmospheric temperature.
	Natural convective heat transfer coefficient [33], h_{conv}	$h_{conv} = 0.557 \times 10^{-6} (\frac{T_R - T_{amb}}{H_T})^{0.25}$ Here, H_T is the height of the solar tower.
	Net heat supplied to power block and storage [33], Q_{net}	$Q_{net} = \alpha_R Q_{in} - (Q_{rad} + Q_{conv}) = Q_{ps} + Q_{sto}$ Here, α_R is absorptivity of the receiver.
	Net energy received [33], Q_{in}	$Q_{in} = \eta_{opt} Q_S$
	Total incident radiation on the heliostats [33], Q_S	$Q_S = DNI \cdot A_h$ Here, A_h is the total area of the heliostats.
Thermal storage	Heat transfer to thermal storage [16], Q_{sto}	$Q_{sto} = M_S C_S (T_b - T_a)$ Here, C_S is the specific heat of molten salt, T_b and T_a are the temperature of hot tank and cold tank respectively.
	Efficiency of thermal storage [16], η_{sto}	$\eta_{sto} = \frac{Q_{ps} + Q_{sto}}{Q_{ps}}$ Q_{ps} is the energy supplied from the central receiver to power block.
Power Block	Turbine [31]	$\eta_T = \frac{h_5 - h_6}{h_5 - h_{6s}}$, $W_T = M_{cf} (h_5 - h_6)$
	HTR [31]	$Q_{HTR} = h_4 - h_3 = h_6 - h_7$
	LTR [31]	$Q_{LTR} = h_7 - h_8 = SR_C (h_3 - h_2)$
	MSHE [31]	$Q_{MSHE} = M_S (h_a - h_b) = M_{cf} (h_5 - h_4)$ M_S is the mass flow of molten salt and h_a and h_b are the inlet and outlet enthalpies of molten salt respectively. Here SR_C is the split ratio between NDDCT and RC.
	MC [31]	$\eta_{MC} = \frac{h_{2s} - h_1}{h_2 - h_1}$, $W_{MC} = SR_C \cdot M_{cf} (h_2 - h_1)$
	RC [31]	$\eta_{RC} = \frac{h_{3s} - h_8}{h_3 - h_8}$, $W_{RC} = (1 - SR_C) M_{cf} (h_3 - h_8)$
	Net power generation [31]	$W = W_T - W_{MC} - W_{RC} - W_p$ W_p is the power consumed by the molten salt pump.
	Cycle efficiency [31], η_{th}	$\eta_{th} = (W_T - W_{MC} - W_{RC} - W_p) / Q_{MSHE}$
	Plant efficiency [31], η	$\eta = (W_T - W_{MC} - W_{RC} - W_p) / Q_{net}$

Two sets of design point air temperature (DP-1 and DP-2) is chosen based on the mean temperature and the highest frequency of air temperature in a specific year. Hence, two dry cooled CSP plant will be designed based on different design point climate temperature. This work emphasizes the design criteria of a dry-cooled CSP plant for optimal thermal performance under various climate conditions.

3.2. Boundary condition at two design point

In sCO₂ power cycles, the turbine exits at a constant pressure (which is different from the Rankine cycle where exit pressure depends on the temperature). The optimum heat rejection is to make the compressor consume a minimum work, which happens near the pseudocritical temperature. Any more heat rejection will require more heat addition in the solar field (boiler in Rankine cycle) which reduces the cycle efficiency. Hence, for the recuperated supercritical CO₂ cycle efficiency, there is a small window near the critical temperature when the marginal addition to the heat loss to the ambient exceeds the marginal benefits gained in the compressor work due to the slightly higher density. This is caused by very high specific heat near the pseudocritical point. This unique mechanism of cooling process near the critical parameters is completely different from those of the cooling in the Rankine cycle/Brayton cycle/any subcritical power cycles. Therefore, the sCO₂ cycle shows the opposite trend of cycle efficiency at lower sink temperature comparing with the Rankine steam cycle. For different turbine exit pressure, there is an optimum lowest temperature until which the efficiency keeps increasing and beyond that temperature, the trend of the curve is a decreasing function of temperature, as shown in Fig. 3. The temperature until which the efficiency increases is a function of cycle lower pressure.

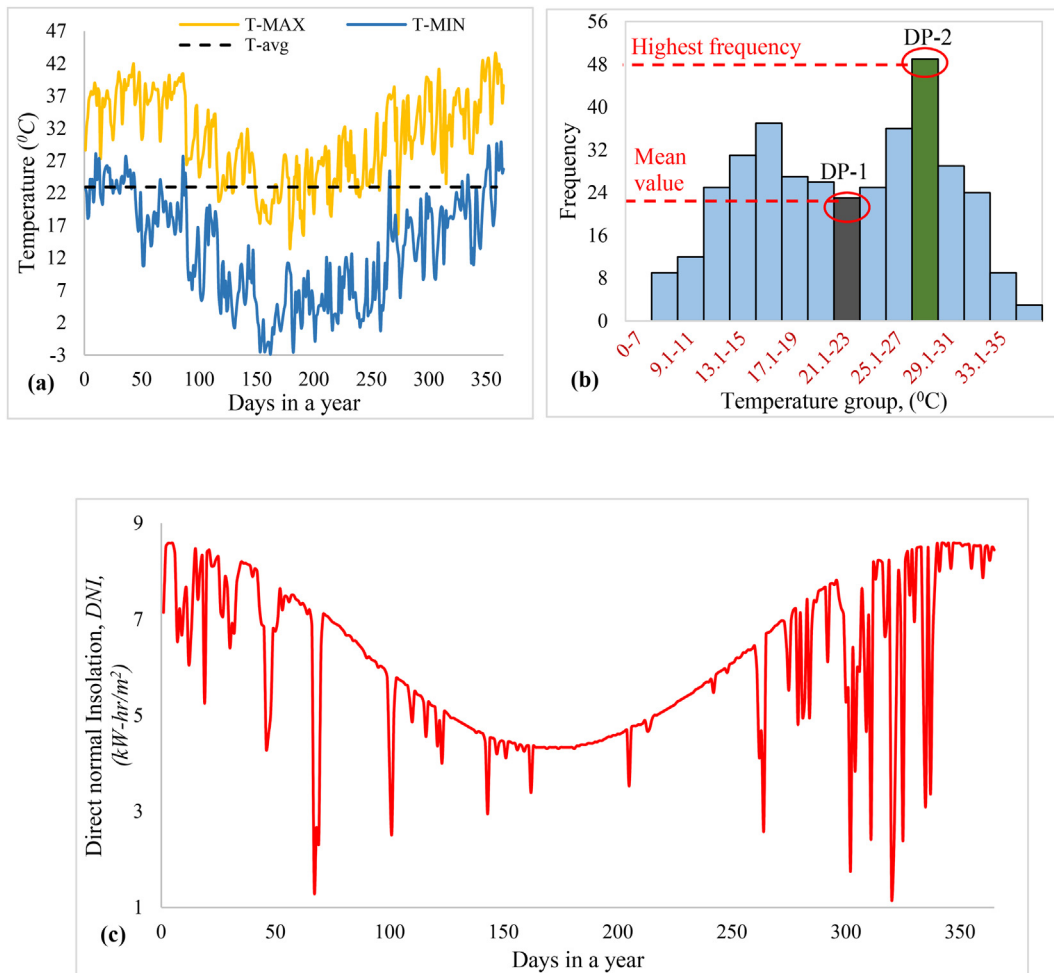


Fig. 2. (a) Annual temperature variation in terms of maximum and minimum daily temperature, (b) frequency histogram of daily mean temperature, (c) fluctuation of year-round solar insolation.

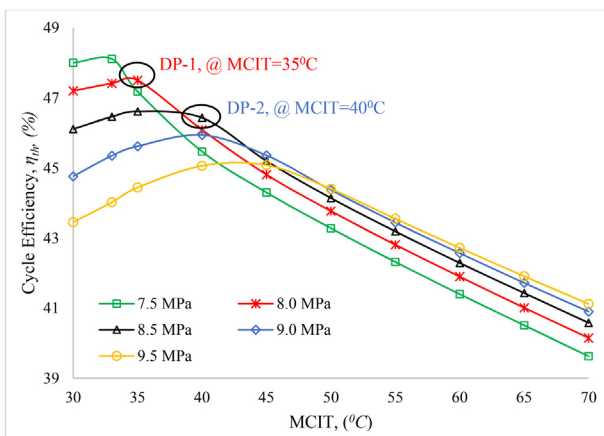


Fig. 3. Evaluation of optimum MCIT with two design points.

The selection of two sets of ambient temperature requires another two sets of MCIT at optimized compressor inlet pressure to design the cooling system. For DP-1 (air = 23 °C), the target MCIT from the cooling tower is selected as 35 °C at 8.0 MPa and for DP-2 (air = 29 °C), the feasible desired MCIT is chosen as 40 °C at 8.5 MPa. The cooling tower should be designed proportionately so that the desired tower exit temperature/MCIT is achieved for both cases (DP-1 & DP-2). Table 2, shows the boundary condition of the solar field and power block for scenarios. Most of the parameters are consistent with the literature

while others (solar filed size, tank capacity, cold tank temperature salt mass flow, and compressor inlet pressure) are optimized (from section 4) prior to the coupling of cooling tower with CSP Plant. Section 5 reveals the design of the CSP plant at the optimized MCIT condition.

4. Designing the dry cooling tower

In NDDCT, the buoyancy force is generated as a result of the temperature change of inside hot humid air and the outside air, shown in Fig. 4. Thermal energy is exchanged between hot sCO₂ inside the tubes of ACHE and fresh inlet air. The mass flow rate of air through the ACHE depends on the air temperature difference and the tower elevation. The choice of various geometric parameters for the cooling system is elaborately discussed in our previous work [28]. The fundamental thermodynamic equations for designing ACHE and NDDCT are taken from ref [34].

The detailed specification of ACHE is prescribed in ref [34] and shown in Fig. 5. The validation of our proposed cooling tower model with a nodal approach applied in the heat exchanger of ACHE inside NDDCT performed in our earlier studies [26,27]. Our previous work also demonstrated the validation of the recompression power cycle simulation results with the literature [8,31,35]. The evaluation of the local heat transfer characteristics, local temperature profile of sCO₂ inside ACHE, pressure drop distribution along the tube as well as across the tube, the draft force and air mass flow rate with a detailed flow chart are comprehensively discussed in our previous work [26,27]. The analysis in section 5 is performed with a simple cooler to rectify an

Table 2
System boundary conditions for designing cooling system.

Solar Field	Parameter	DP-1	DP-2
	Direct solar irradiance, DNI	6.1 kW-hr/m ²	6.1 kW-hr/m ²
	Reflectivity of the heliostat	0.9	0.9
	Cleanliness of heliostat	0.97	0.97
	Radiative shape factor, F_{view}	1	1
	Convective heat loss factor, f_{conv}	1	1
	Absorptivity of central receiver, α_R	0.9	0.9
	Absorptivity of thermal insolation, α_{th}	0.95	0.95
	Heliostat length and width	10 × 10	10 × 10
	No of heliostat, N	3266	3474
	Heliostat field area	326600 m ²	347400 m ²
	Total incident radiation on the heliostats, Q_S	166.6 MW	177.5 MW
	Net energy received, Q_{in}	116.6 MW	124.2 MW
	Net heat supplied to power block and storage, Q_{net}	104.9 MW	111.8 MW
	Maximum allowable temperature of hot salt	590 °C	590 °C
	Molten salt split ratio, SR_s	50%	50%
	Salt mass flow rate, M_S	468.6 kg/s	565.4 kg/s
	Pressure drop in receiver	50 kPa	50 kPa
	Tank capacity of 8 h	6.74 × 10 ⁶ kg	8.14 × 10 ⁶ kg
	Tank capacity of 10 h	8.43 × 10 ⁶ kg	10.17 × 10 ⁶ kg
	Tank capacity of 12 h	10.11 × 10 ⁶ kg	12.21 × 10 ⁶ kg
Power Block	Plant electrical output, W	25 MW	25 MW
	Turbine adiabatic efficiency, η_T	0.93	0.93
	RC adiabatic efficiency, η_{RC}	0.89	0.89
	MC adiabatic efficiency, η_{MC}	0.89	0.89
	Turbine rotational speed	60,000	60,000
	Compressor rotational speed	5,000	5,000
	Generator efficiency	0.9	0.9
	Motor efficiency	1.0	1.0
	Mechanical effectiveness, η_M	1.0	1.0
	Cycle fluid split ratio, SR_C	62.7% (optimised)	59.4% (optimised)
	Cycle fluid mass flow rate, M_{cf}	290.7 kg/s	350.8 kg/s
	Hot salt temperature	580 °C	580 °C
	Cold tank temperature	435 °C (optimised)	450 °C (optimised)
	Pinch point in MSHE	5 °C	5 °C
	Inlet temperature of NDDCT	67.5 °C	107.3 °C
	Desired cycle lowest temperature	35 °C (optimised)	40 °C (optimised)
	Environmental conditions	60% RH, 1 m/s, 0.1 MPa	60% RH, 1 m/s, 0.1 MPa
	Turbine inlet pressure, P_H	20 MPa	20 MPa
	Turbine exhaust pressure, P_L	8 MPa (optimized)	8.5 MPa (optimized)
	Pinch point temperature in LTR	5 °C	5 °C
	Pressure drop in HTR and LTR	20 kPa	20 kPa

optimal working condition in terms of MCIT and cycle fluid inlet temperature in the tower and reveals the required size of the NDDCT for both cases. Finally, **section 6** demonstrates the dynamic performance assessment of both CSP plants coupled with NDDCT designed against two different climate temperatures.

5. Numerical solution procedure

The system (central receiver + power cycle + NDDCT) simulation is performed with IPSEpro [36]. The typical cooling system component in IPSEpro fails to account for local property variation of supercritical fluids in the ACHE bundles inside the tower. Therefore, the model development kit (MDK) is employed to design the tower using model development language. The robust optimization algorithm is applied while solving the mathematical equations in all the components. The system is iteratively computed to maintain the pinch point constraint in the LTR and boundary conditions applied in other components. Also, other test conditions (mass balance, temperature crossover in the recuperators, MSHE, and ACHE) are checked by the code after each iteration. Fig. 6 shows a flow chart which demonstrates the numerical solution procedure applied in the present analysis. The sCO₂ property variation requires special treatment in modelling the ACHE inside the tower and recuperators. This is addressed by implementing the nodal approach in each small segment with the discretization of ACHE and recuperator.

The attention is paid in both sCO₂ and airside property changes while discretizing the heat exchangers. The local heat transfer

coefficient for sCO₂ is determined by Yoon et al. correlation [37] applicable for macro tube geometries. In most of the works found in literature, the heat exchanger discretized with fixed geometric dimensions. This is not the case in the present analysis, where the required number of ACHE bundles has been estimated after achieving the design requirements of the cooling tower. Moreover, the heat exchangers are placed inside NDDCT. The complex interaction of the heat exchanger characteristics, the tower dimensions and the buoyant force for the evaluation of draft force are the challenging issues in designing the NDDCT. The required specification of the NDDCT for two design points is demonstrated in the next section.

6. Designing CSP at optimum MCIT condition

The CSP plant is designed based on the optimum NDDCT outlet temperature/MCIT. This section demonstrates how different parameters (heliostat numbers, hot and cold tank temperature, salt mass flow rate, solar salt ratio, and tank capacity) of the CSP field are evaluated and optimized (cold tank temperature and solar salt mass flow). This part of modelling is performed with a standard cooler model to rectify the optimal working conditions of the power block and solar field before integrating the cooling tower. Once various parameters of the solar field are optimized (see Table 2) then it is integrated with the detailed model of a dry cooling tower to perform the yearlong thermal performance of the dry cooled CSP plant for two scenarios, which is elaborately discussed in the next section.

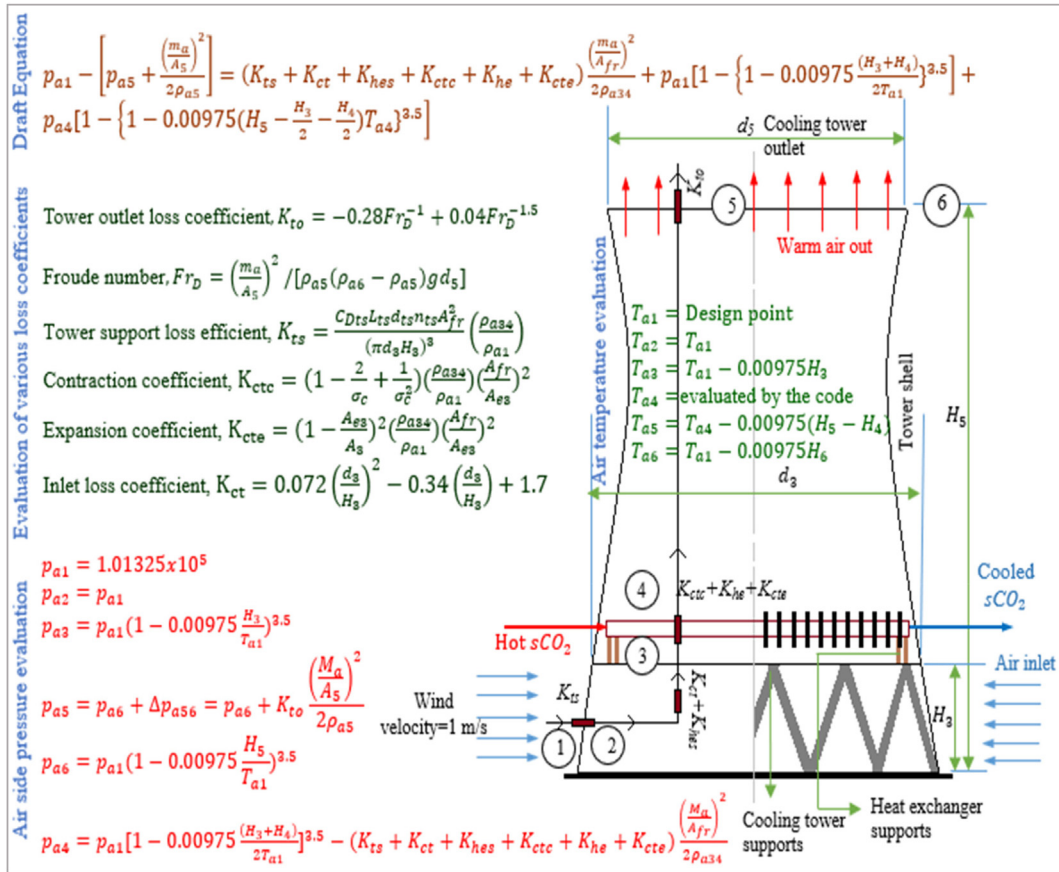


Fig. 4. Detailed view of NDDCT with the model equations.

6.1. Sizing the heliostat field

The required size of the solar field at two design-point MCIT is demonstrated in Fig. 7. Increasing the number of heliostats enhances the net power, *W* for both cases. However, an optimal point of the CSP plant efficiency, η is observed beyond which the heat supplied from the central receiver with the higher number of heliostats exceeds the marginal increase in *W*. The required mass flow of molten salt, *M_s* and cycle fluid, *M_{cf}* with the variation of solar field size is depicted in Fig. 8. Both parameters linearly increase with the increase of the heliostat field and then show no significant changes once the optimal point is reached where the plant efficiency is maximum. However, at DP-2, the CSP plant requires higher values of solar salt mass flow and sCO₂ mass flow compared to the CSP plant designed at DP-1 due to the increased compressor inlet pressure.

6.2. Selection of hot salt and cold tank temperature

The improvement of both plant efficiency and cycle efficiency with the increase of solar salt temperature attained in the central receiver is shown in Fig. 9. Since the maximum temperature of the nitrate salt is limited to 590 °C, hence to avoid the boiling issues and for safety concerns in the TES, the temperature of the hot tank is considered as 580 °C with 5 °C pinch in the MSHE. The cold tank temperature (435 °C at DP-1 and 450 °C at DP-2) at two design-point is selected based on the highest cycle efficiency as shown in Fig. 10. The cycle efficiency merely increases and then drops quickly with higher cold tank temperature. At higher cold tank temperature values, the temperature of the sCO₂ stream entering the MSHE decreases which requires more heat addition from the central receiver. The salt mass flow remains unchanged at higher cold tank temperature.

6.3. Evaluation of tank capacity

The CSP plant has been designed with a 12-hour charging capacity of TES. The molten salt mass flow increases with the tank capacity, as shown in Fig. 11. At lower tank capacity, the TES requires a lower amount of salt to be stored in the hot tank, hence the more solar salt is available in the MSME to exchange the heat. The tank capacity is evaluated for 25 MW thermal output. At higher tank capacity, the salt mass flow insignificantly increases which requires more solar salt to be stored in the TES for the same charging capacity. The net power, *W* drops since a lower amount of solar salt is supplied in the MSHE when tank capacity increases from the required value. At DP-2, the TES capacity is higher than DP-1, since higher sCO₂ mass flow for DP-2 requires higher solar salt to maintain all the boundary conditions prescribed for both plants.

6.4. Sizing the cooling tower

Based on the optimum working conditions obtained from the previous section, the simple cooler model is now replaced with detailed NDDCT. The required size and specification of the tower for both CSP plant is demonstrated in Fig. 12 designed against two different climate temperatures (23 °C and 29 °C) to attain the desired MCIT (35 °C for DP-1 and 40 °C for DP-2) respectively. Although the desired MCIT for DP-2 is lower, still it requires a taller NDDCT (67 m for DP-2, 59 m for DP-1). This is due to the requirement of higher sCO₂ mass flow entering into the tower, which requires more ACHE bundles (*N_b* = 36 for DP-2 and *N_b* = 28 for DP-1) to cool the working fluid. The common geometric relations of tower design are prescribed. The tower off-design performance at different climate conditions (air temperature and DNI) will change the MCIT/tower exit temperature which will significantly

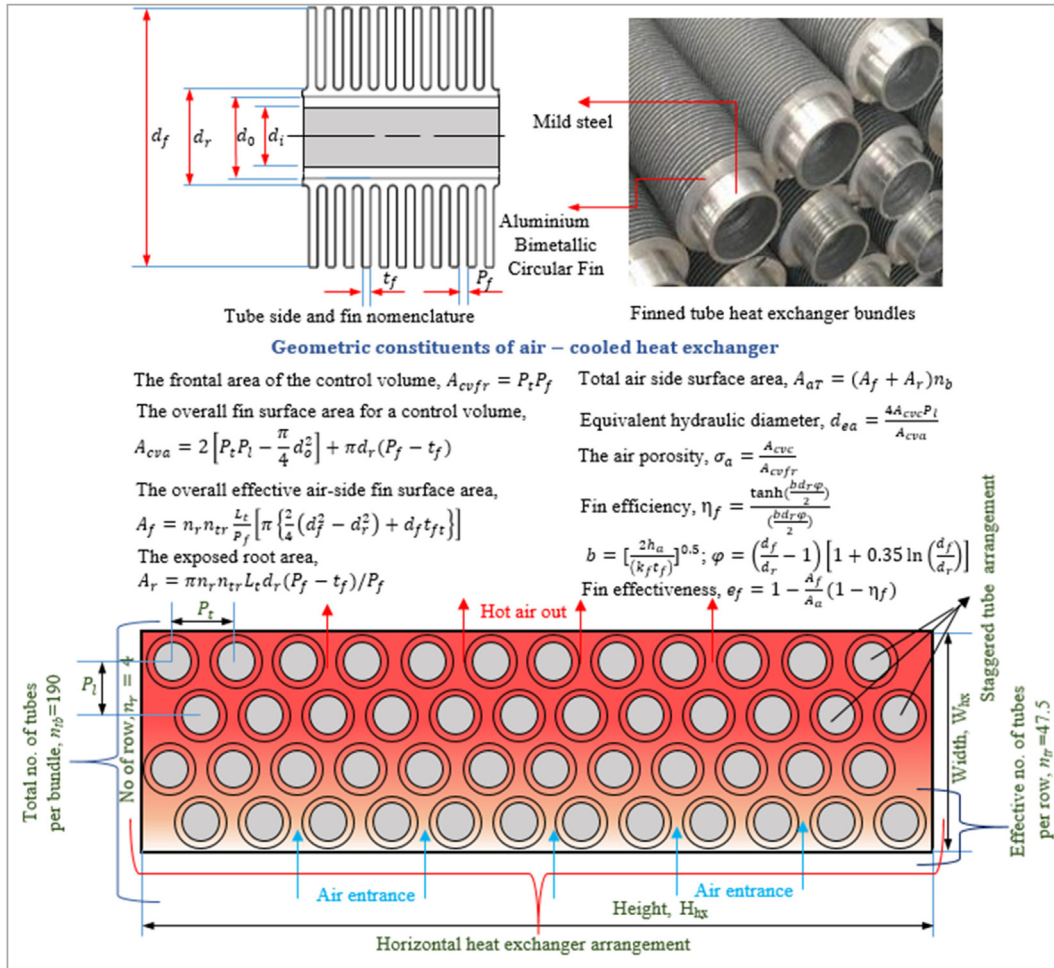


Fig. 5. The geometric constituents of ACHE with a complete definition of nomenclature.

impact the plant performance during daytime as well as nighttime operation with TES.

7. Results

7.1. Utilization of additional bypass at Off-design condition

The advantage of additional bypass (BP) arrangement prior to NDDCT in the occasion of low ambient temperature period is demonstrated in Fig. 13. Without this supplementary BP, both CSP plants experience overcooling when the ambient temperature is below the design point (23 °C for DP-1 and 29 °C for DP-2). The lower the ambient air, the higher the sCO₂ mass flow bypassing the NDDCT. The CSP plant designed at DP-2 offers maintaining a constant MCIT over a wide range of air temperatures since the NDDCT is designed against a higher ambient temperature. The usage of BP allows operating both plants at the supercritical state and any compressor issue working under subcritical condition is thus avoided with this approach. The BP arrangement is not activated during higher ambient temperatures; however, the split ratio of the cycle is varied for optimized operation. The year-round NDDCT off-design performance is shown in Fig. 14(a).

Since the tower size is higher for DP-2, it requires higher air mass flow rate and heat rejection. The average heat rejection in NDDCT is 27.05 MW and 29.1 MW, whereas the average air mass flow is 1426 kg/s and 1775 kg/s respectively. The activation of BP throughout the year for both plants is shown in Fig. 14(b) and 14(c). In the case of DP-1, during the daytime (from 7:00 to 19:00) of summer, autumn and spring, the BP is turned off for most of the occasions since the ambient

temperature is quite higher than the design point. During winter, the air temperature is always lower, hence the BP activates throughout the 24-hour period thus preventing the cycle from overcooling and maintaining optimal performance at a lower temperature period. The BP activates for most of the occasions for DP-2 as compared to DP-1.

7.2. Year-round TIT, cold tank and MCIT observation

The intermittent nature of DNI stimulates substantial variation in the turbine inlet temperature, TIT for both CSP plants. On the occasions when the DNI is higher than the design value (6.1 kW-hr/m²), both plants maintain the highest limit of TIT = 575 °C to maximize power generation. In the case of low DNI periods, the molten salt mass flow rate in the central receiver decreases. Since the TES are designed for 12-hr capacity, the central receiver ensures the complete charging of TES by maintaining a constant mass flow of molten salt flowing into the hot tank regardless of the DNI conditions. As a consequence, during low DNI periods, the portion of molten salt flowing into the power block (through MSHE) decreases. The reduced salt mass flow adversely impacts the TIT due to the reduction of heat transfer in the MSHE, as portrayed in Fig. 15. The variation of year-round cold tank temperature with the change of climate condition is depicted in Fig. 16. The higher the DNI value, the lower the cold tank temperature in the TES as a result of increased heat transfer in the MSHE. At lower DNI values, the impaired heat transfer in MSHE increases the cold tank temperature.

The year-round MCIT/tower exit temperature variation evaluated with mean air temperature and maximum ambient temperature is shown in Fig. 17. It is obvious that the additional BP allows operating

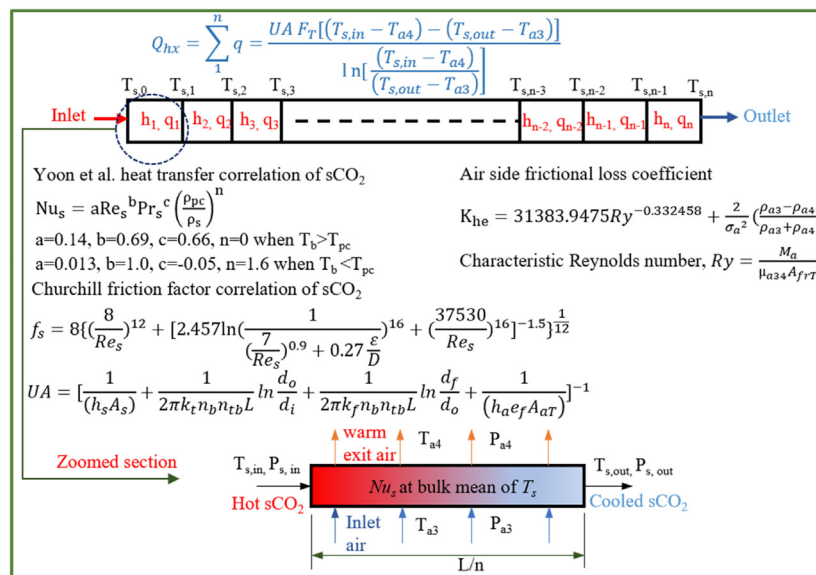
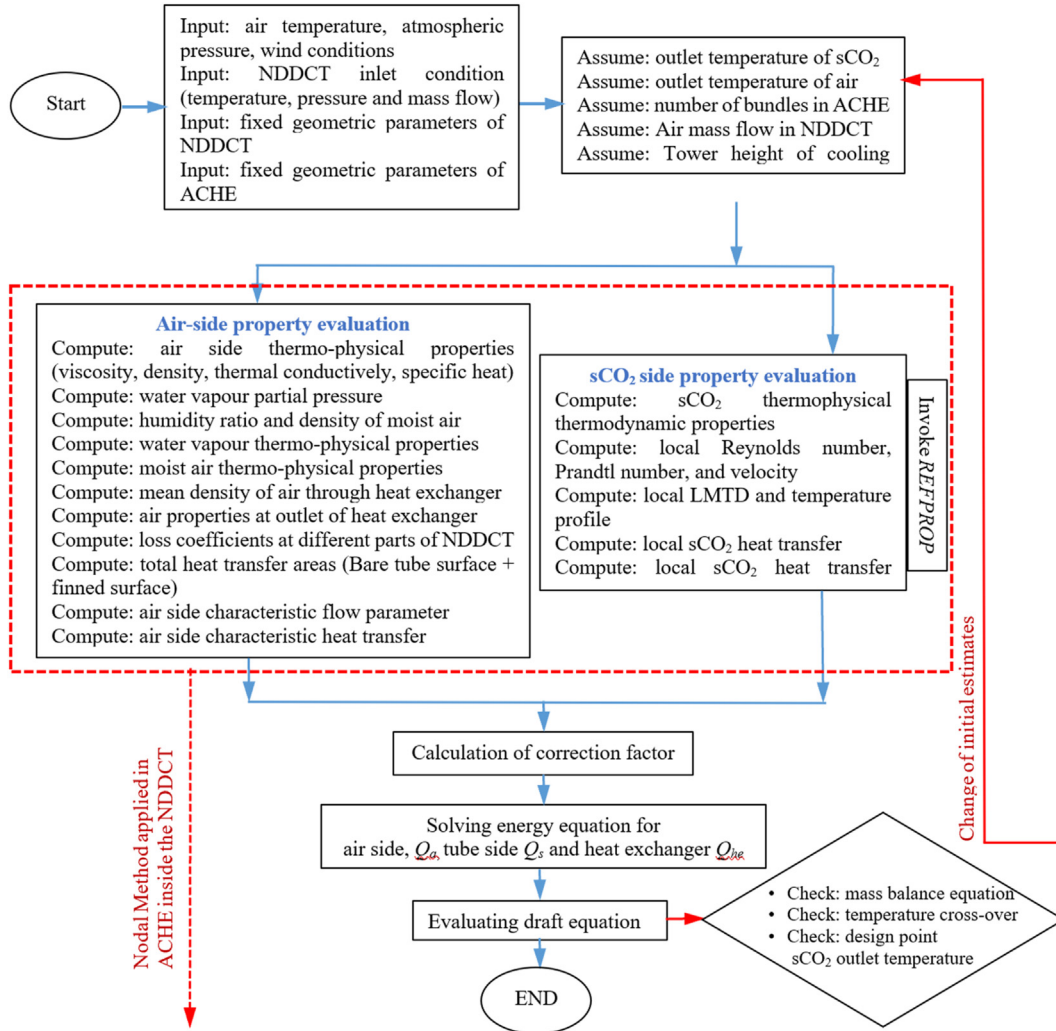


Fig. 6. Flow chart demonstrating the numerical simulation procedure to design the NDDCT.

the plant to preserve the design point MCIT for optimized operation. However, the annual maximum air temperature dataset shows more fluctuation in MCIT values since the towers are designed against mean ambient temperature. Controlling the MCIT does not guarantee for maximum power generation since the CSP plant performance is also

governed by the DNI fluctuation.

7.3. Year-round performance comparison

The year-round CSP plant performance by the influence of both DNI

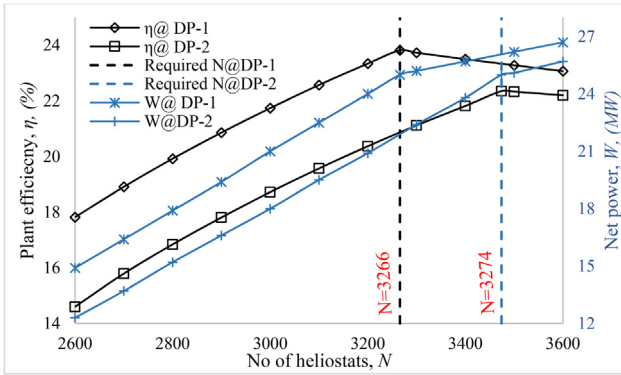


Fig. 7. Sizing the heliostats at two design point conditions based on optimum plant efficiency.

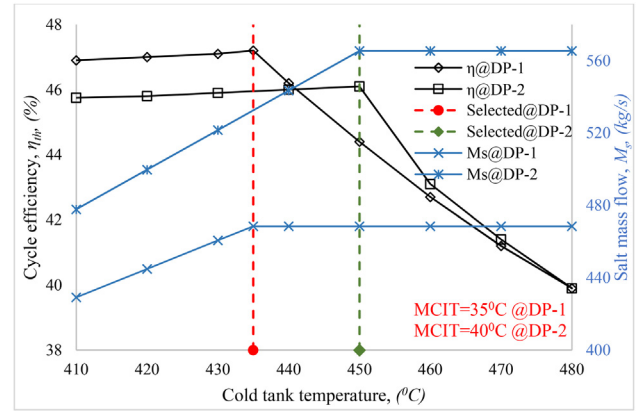


Fig. 10. Selection of cold tank temperature for two design point MCIT conditions.

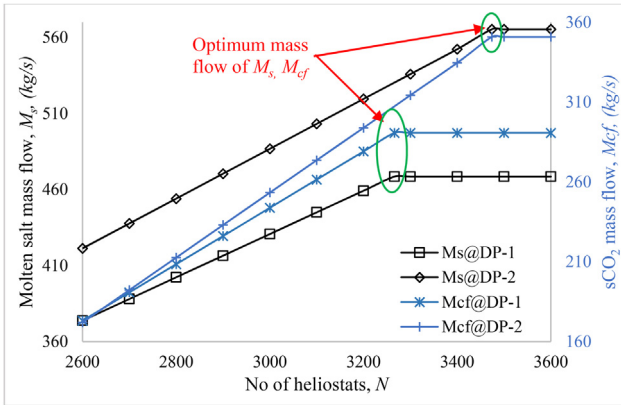


Fig. 8. Variation of molten salt and sCO₂ mass flow with respect to the heliostat field.

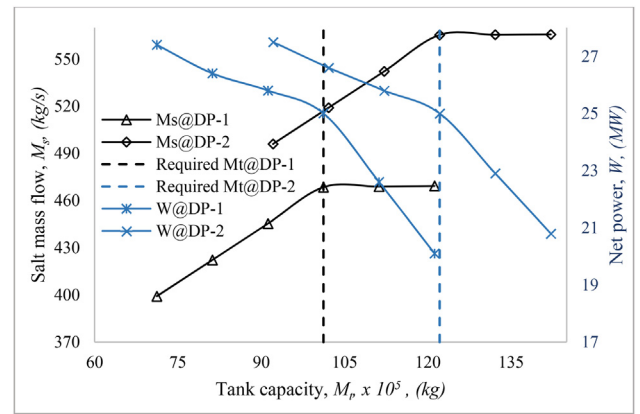


Fig. 11. Evaluation of tank capacity for thermal energy storage of capacity 12 h.

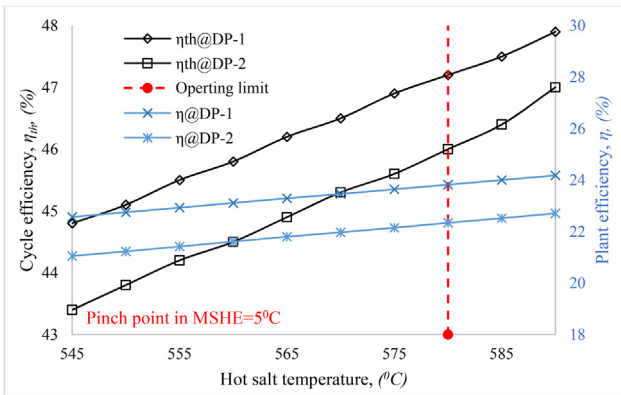


Fig. 9. Selection of hot salt temperature for two design point MCIT conditions.

and ambient air is shown in Fig. 18 using the minimum, mean, and maximum temperature dataset. The CSP plant designed against DP-2 shows superior performance in terms of net power production in comparison with DP-1. At DP-2, the plant shows more stability by preserving the required MCIT on most of the occasions. However, this comes at the expense of taller NDDCT and increased the capital cost of the solar components. Thus the proper selection of ambient air to design the tower for CSP plant is imperative for economic operation. The average net power using the minimum climate temperature for DP-1 and DP-2 is 23.71 MW and 24.09 MW respectively, whereas using the maximum climate temperature the values are 23.06 MW and 23.45 MW. This power generation takes account of TES of capacity 12 hr working during nighttime for uninterrupted electricity production.

However, for more precise prediction of power generation in particular with TES technology, an hourly climate temperature dataset are necessary which are explained in the following section.

7.4. TES working mechanism

This section comprehensively demonstrates the TES working mechanism. The mass flow of sCO₂ is always kept constant regardless it is daytime or nighttime. The fixed inventory of sCO₂ provides easier operation of the plant. However, this is not the case for the solar salt inventory system. The working mechanism of TES for dry-cooled sCO₂ CSP plant is explained using the hourly climate temperature dataset. During the daytime, the TES is kept in operation by charging. A portion of the total mass of molten salt (salt split ratio) is stored in the hot tank while the remaining amount is delivered in the power block. While the DNI value fluctuates in every hour, the salt split ratio is also varied ensuring the complete charging of TES for 12 hr. Hence, the salt mass flowing into the power block varies with DNI while the amount flowing into the TES is kept the same (234.3 kg/s) regardless of the climate condition. Hence, the turbine inlet temperature significantly varies during the daytime. At nighttime, when no solar energy is accessible, the TES starts its discharging mode by delivering the hot salt to the power block. As if the plant is working under a constant DNI condition with only disturbance to the system is ambient temperature. A more stable power generation is expected from the proposed CSP plants while working under TES since the salt mass flowing into the power block in now constant. This allows maintaining a constant turbine inlet temperature during nighttime. However, the ambient temperature also changes during nighttime which can be counterbalanced by activating

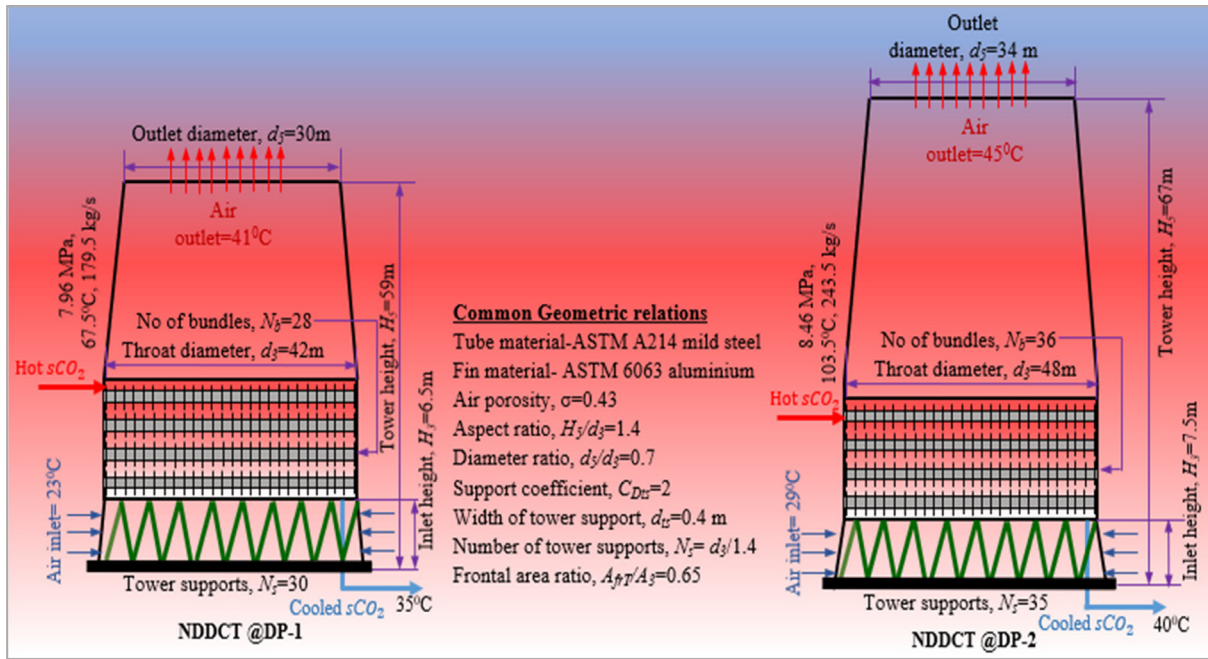


Fig. 12. The required size of NDDCT for both CSP plants designed at different air temperature.

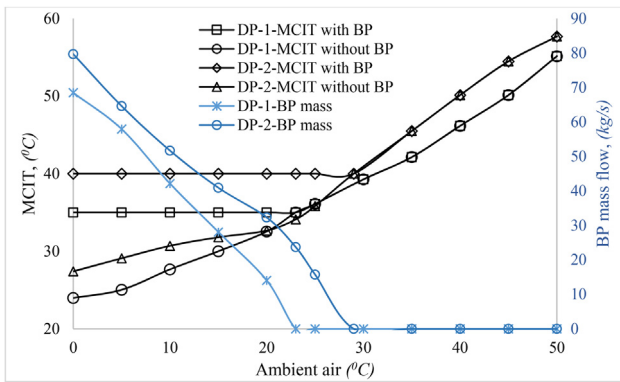


Fig. 13. Mechanism of additional flow bypass arrangement for optimal performance.

the additional bypass arrangement. This bypass regulates the sCO₂ mass flow into the NDDCT only on the occasion of lower ambient temperature. Fig. 19 demonstrates the TES working mechanism in terms of variation of solar salt for a typical winter day.

The earlier sections suggest better performance for the CSP plant designed against DP-2, hence the results on the TES working mechanism is elucidated for this plant only. At various seasonal conditions (summer, autumn, winter, and spring), the hourly power generation for CSP plant during daytime and nighttime is demonstrated in Fig. 20 under variant climate conditions. It is challenging to obtain a firm conclusion on which season the CSP plant shows the highest thermal performance. Hence, a typical day in each season is chosen to elucidate the variation in plant performance complemented with TES and additional NDDCT flow splitter.

In a typical summer day, the additional flow splitter activates only during nighttime when the air temperature is below 29 °C and varies between 9.1 and 14.1%. The daytime temperature is always higher than the design point, hence the main flow splitter changes the split ratio to maximize the power generation. In autumn, the NDDCT flow splitter activates for the whole period of time as the air temperature is always lower than the design point. Similar performance is observed during winter and spring, however, during winter the bypass fraction shows a

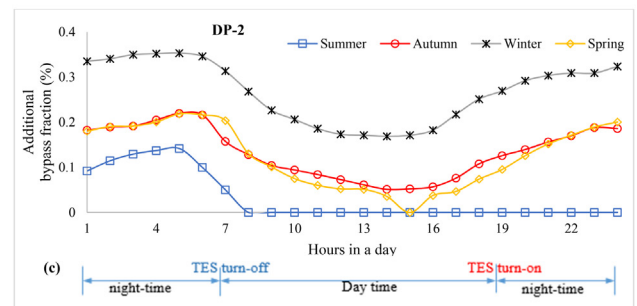
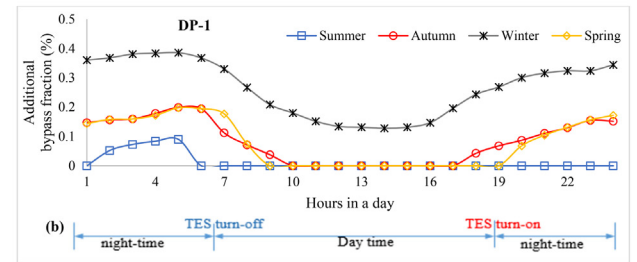
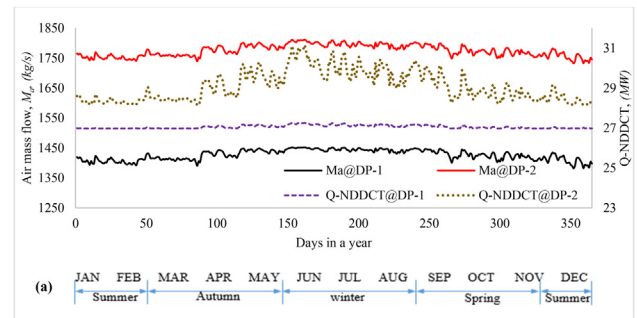


Fig. 14. (a) The NDDCT off-design performance. The usage of additional bypass arrangement at a temperature lower than the design point is shown for two proposed plant (b) design point-1, (c) design point-2.

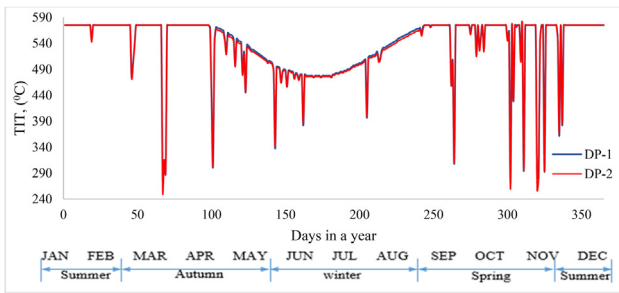


Fig. 15. Annual TIT variation with the variation of DNI.

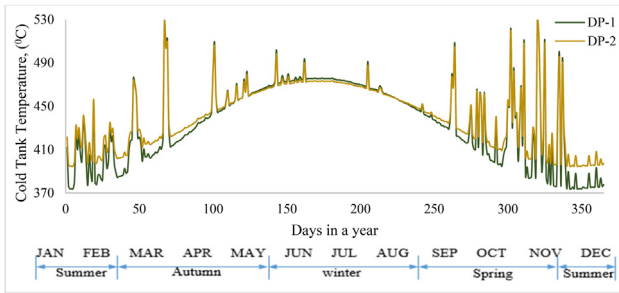


Fig. 16. Cold tank temperature variation in variant climate condition.

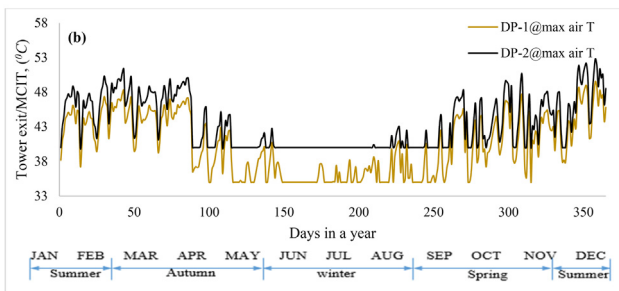
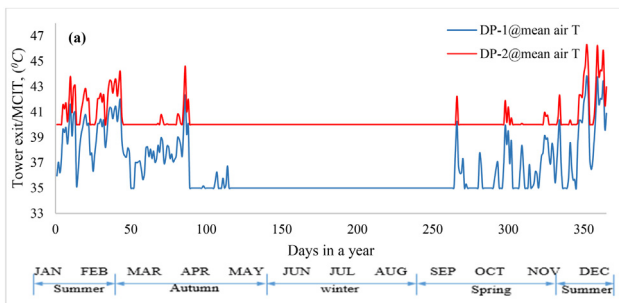


Fig. 17. Annual MCIT variation at two design-point with respect to daily (a) mean air temperature and (b) maximum air temperature.

significant variation (17.1–35.2%) due to very low ambient temperature. The main flow splitter remains almost constant (61.4%) during autumn, winter, and spring. At 7:00 in the morning, the TES is turned off and the plant operates with the available solar energy. The variation in solar energy alters the turbine inlet temperature which consequently impairs power generation. Moreover, the portion of solar salt flowing from the central receiver to the power block always changes with DNI. Nevertheless, the sCO₂ cycle operates under a fixed inventory system regardless of the climate conditions.

The molten salt mass flow is a dominant parameter that shows continuous fluctuation under the intermittent nature of solar energy. At 19:00 in the evening when no solar energy is accessible, the TES starts

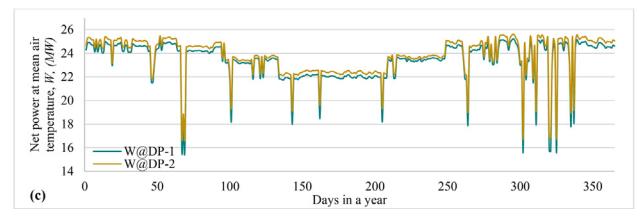
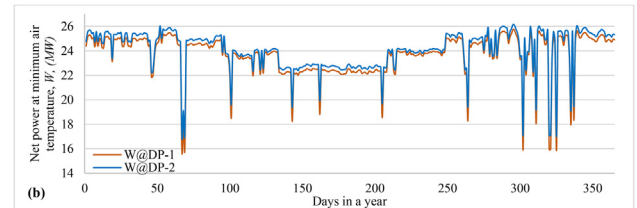
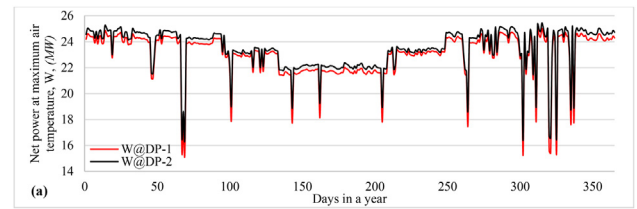


Fig. 18. Year-round plant performance comparison in terms of net power generation using (a) maximum air temperature, (b) minimum air temperature, and (c) mean air temperature dataset.

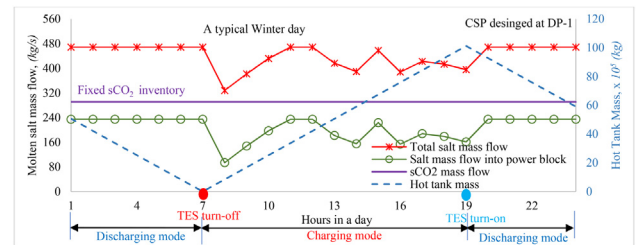


Fig. 19. The working mechanism of TES in terms of the variation of molten salt mass flow.

its discharging mode by utilizing the molten salt stored in the hot tank. A more stable power generation is observed during all seasonal conditions. This is due to the constant supply of solar salt to the power block which helps to operate the plant near the design condition. During the nighttime, the only disturbance parameter is ambient temperature which is counterbalanced by the activation of additional NDDCT flow splitter. The CSP plant designed against DP-1 shows more unsteadiness in the power generation working under TES since the NDDCT is designed against a lower ambient temperature. The mean power generation in a typical day during summer, autumn, winter, and spring are 24.3 MW, 24.1 MW, 21.8 MW, and 25.1 MW respectively. The values are less for the CSP plant designed against DP-1 since the activation frequency of NDDCT flow splitter is less than DP-2. The above figure does not essentially evaluate the best seasonal climate for maximized power generation since for other days in each season, the performance shows considerable variation. Hence, this section emphasizes the TES working mechanism and dynamic attributes of a dry-cooled CSP plant.

In the steam cycle, the lower the cycle minimum temperature, the greater the thermal efficiency. Conversely, this is not applicable for

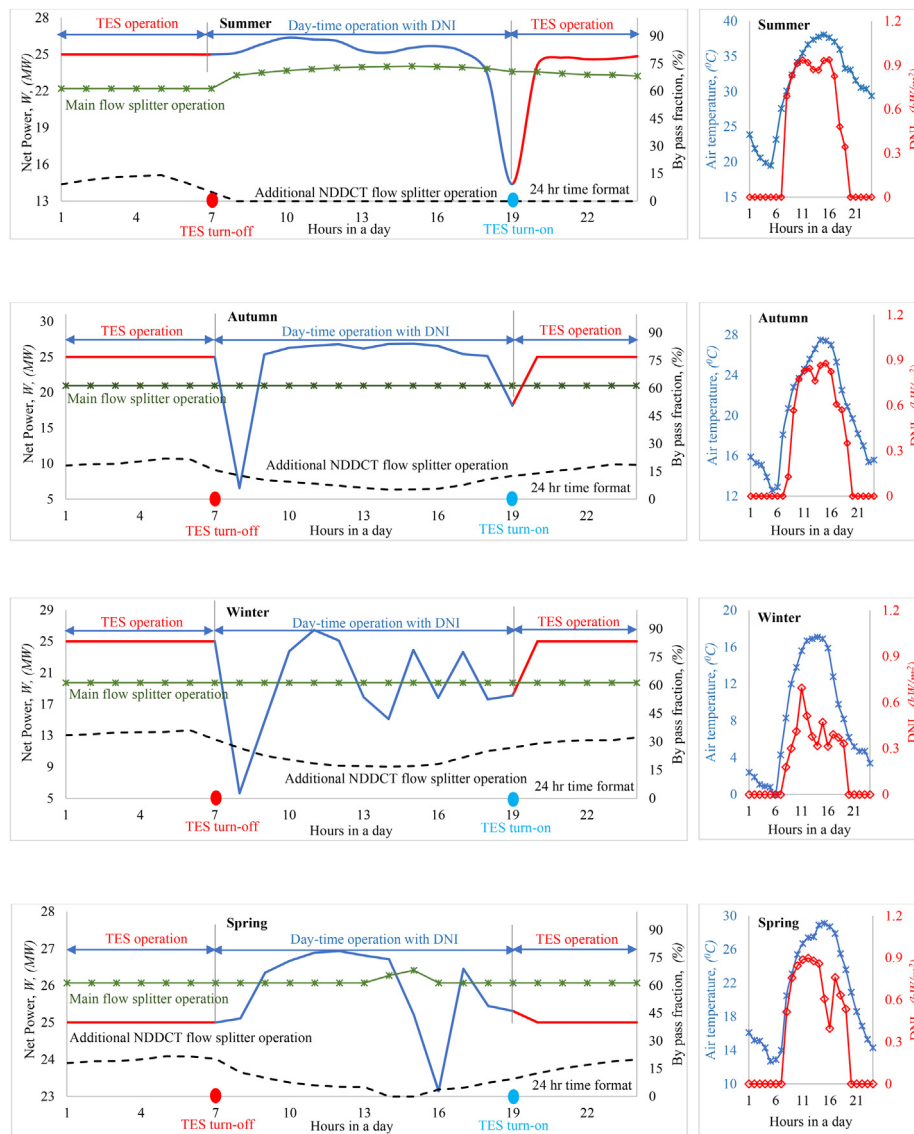


Fig. 20. Hourly CSP plant performance supplemented with TES at various seasonal climates.

sCO₂ power cycles, where cooling the working fluid below the pseudocritical temperature can be extremely problematic for the efficient operation of the compressor. Moreover, our previous research suggests that in a colder environment, the sCO₂ power cycle requires more heat input to the cycle. For CSP application, this requires a larger solar field to provide more thermal energy from the central receiver to operate the power cycle at lower climate temperatures. The subcritical operation of the sCO₂ power cycle is effectively avoided in the present analysis. The subcritical operation of the sCO₂ power cycle generates instabilities in operating the compressors. The additional bypass in the present work carefully addresses this issue by preventing cycle overcooling.

8. Design recommendation for future commercialization

The location of the future CSP plant with sCO₂ power block is greatly suited in a dry climate with high solar irradiance where abundant water supply is truly scarce. The exclusive features of the sCO₂ power cycle like the compactness in the heat exchangers and turbomachineries and preserving superior efficiency at higher climate temperatures with dry cooling can further economize the capital cost of the CSP plant. The adequate selection of ambient temperature to design the cooling tower is crucial for a specific CSP

location, an economic assessment is necessary to obtain an optimal ambient temperature to maximize plant performance. This air temperature should be in between the value of mean temperature and temperature of the highest frequency based on the climate dataset to maximize the annual CSP performance. The detailed economic analysis and optimization of dry cooled sCO₂ power cycles designed against various climate conditions in CSP application is our future research goal.

9. Conclusion

In the present work, the power block is equipped with molten salt thermal energy storage to supplement uninterrupted power generation when no solar insolation is available. The key findings are summarized below.

- Various parameters in the solar system (molten salt mass flow rate, salt split ratio, and cold tank temperature) and the power block (sCO₂ mass flow, bypass fractions, and turbine exhaust pressure) are optimized before designing the cooling tower.
- The required size of the heliostat field, tank capacity of TES, and detailed specification (tower outlet height, tower diameters, number

of heat exchanger bundles, and number of tower supports) of the NDDCT are revealed at optimum MCIT condition. The heat exchangers are discretized for the precise calculation of sCO₂ properties with the change of temperature in the cooling tower as well as in the recuperators.

- As expected, the dry-cooled sCO₂ plant designed with the consideration of the highest frequency of air temperature demonstrates better thermal performance in comparison with the CSP plant designed with average air temperature. However, this comes by the expense of higher requirement of mass flow rate (sCO₂ and molten salt) and higher capital cost in designing the cooling tower and solar field.
- The additional bypass located prior to the NDDCT ensures the plant operates at the design point MCIT to maximize the power generation for the occasion of lower climate temperatures. This bypass prevents the cycle overcooling by reducing the heat dissipation in the NDDCT and ensures the cycle operates in supercritical state at any given climate condition.
- The year-round system dynamic behavior is observed in terms of tower exit temperature, heat rejection in the tower, air mass flow rate, and net power generation under the variant solar insolation and climate temperature. The average net power generation using the minimum air temperature for DP-1 and DP-2 is 23.71 MW and 24.09 MW respectively, whereas for maximum climate temperature the values are 23.06 MW and 23.45 MW.
- The contribution of TES during nighttime and the corresponding system dynamic response is also investigated. The work demonstrates the significance of dry-cooling system design parameters on the CSP plant and its off-design performance under various climatic conditions on the overall system performance. The supplementary bypass of sCO₂ prior to NDDCT is extremely a useful technique to maintain the cycle optimal performance at lower climate temperatures.

CRedit authorship contribution statement

M. Monjurul Ehsan: Conceptualization, Software, Methodology, Investigation, Validation, Writing - original draft. **Zhiqiang Guan:** Writing - review & editing. **Hal Gurgenci:** Resources, Supervision. **Alexander Klimenko:** Supervision.

Declaration of Competing Interest

The authors declare that they have no known competing financial interests or personal relationships that could have appeared to influence the work reported in this paper.

Acknowledgment

Appreciations to the University of Queensland for granting the Research Training Program scholarship. This research has been conducted for Australia Solar Thermal Research Initiative (ASTRI), a project governed by Australia Renewable Energy Agency (ARENA).

References

- [1] Dowling AW, Zheng T, Zavala VM. Economic assessment of concentrated solar power technologies: a review. *Renew Sustain Energy Rev* 2017;72:1019–32.
- [2] Li M-J, Zhu H-H, Guo J-Q, Wang K, Tao W-Q. The development technology and applications of supercritical CO₂ power cycle in nuclear energy, solar energy and other energy industries. *Appl Therm Eng* 2017;126:255–75.
- [3] Duniam S, Jahn I, Hooman K, Lu Y, Veeraragavan A. Comparison of direct and indirect natural draft dry cooling tower cooling of the sCO₂ Brayton cycle for concentrated solar power plants. *Appl Therm Eng* 2018;130:1070–80.
- [4] Garg P, Srinivasan K, Dutta P, Kumar P. Comparison of CO₂ and steam in trans-critical Rankine cycles for concentrated solar power. *Energy Procedia* 2014;49:1138–46.
- [5] Persichilli M, Klaculis A, Zdankiewicz E, Held T. Supercritical CO₂ power cycle developments and commercialization: why sCO₂ can displace steam ste. *Power-Gen India & Central Asia* 2012.
- [6] Cheng L. Evaluation of Correlations for Supercritical CO₂ Cooling Convective Heat Transfer and Pressure Drop in Macro-and Micro-Scale Tubes. *Int J Microsc Nanosc Therm Fluid Transp Phenom* 2014;5(2):113.
- [7] Ehsan MM, Guan Z, Klimenko A. A comprehensive review on heat transfer and pressure drop characteristics and correlations with supercritical CO₂ under heating and cooling applications. *Renew Sustain Energy Rev* 2018;92:658–75.
- [8] Besarati SM, Goswami DY. Analysis of advanced supercritical carbon dioxide power cycles with a bottoming cycle for concentrating solar power applications. *J Sol Energy Eng* 2014;136(1):010904.
- [9] Dyreby J, Klein S, Nellis G, Reindl D. Design considerations for supercritical carbon dioxide Brayton cycles with recompression. *J Eng Gas Turbines Power* 2014;136(10):101701.
- [10] Wright SA, Radel R, Conboy T, Rochau GE. Modeling and Experimental Results for Condensing Supercritical CO₂ Power Cycles. Sandia Report 2011.
- [11] Marchionni M, Bianchi G, Tsamos KM, Tassou SA. Techno-economic comparison of different cycle architectures for high temperature waste heat to power conversion systems using CO₂ in supercritical phase. *Energy Procedia* 2017;123:305–12.
- [12] Cao Y, Ren J, Sang Y, Dai Y. Thermodynamic analysis and optimization of a gas turbine and cascade CO₂ combined cycle. *Energy Convers Manage* 2017;144:193–204.
- [13] Kim S, Cho Y, Kim MS, Kim M. Characteristics and optimization of supercritical CO₂ recompression power cycle and the influence of pinch point temperature difference of recuperators. *Energy* 2018;147:1216–26.
- [14] Zhu H-H, Wang K, He Y-L. Thermodynamic analysis and comparison for different direct-heated supercritical CO₂ Brayton cycles integrated into a solar thermal power tower system. *Energy* 2017;140:144–57.
- [15] Wang K, He Y-L. Thermodynamic analysis and optimization of a molten salt solar power tower integrated with a recompression supercritical CO₂ Brayton cycle based on integrated modeling. *Energy Convers Manage* 2017;135:336–50.
- [16] Wang K, Li M-J, Guo J-Q, Li P, Liu Z-B. A systematic comparison of different S-CO₂ Brayton cycle layouts based on multi-objective optimization for applications in solar power tower plants. *Appl Energy* 2018;212:109–21.
- [17] Padilla RV, Too YCS, Benito R, Stein W. Exergetic analysis of supercritical CO₂ Brayton cycles integrated with solar central receivers. *Appl Energy* 2015;148:348–65.
- [18] Singh R, Miller SA, Rowlands AS, Jacobs PA. Dynamic characteristics of a direct-heated supercritical carbon-dioxide Brayton cycle in a solar thermal power plant. *Energy* 2013;50:194–204.
- [19] Osorio JD, Hovsapian R, Ordóñez JC. Dynamic analysis of concentrated solar supercritical CO₂-based power generation closed-loop cycle. *Appl Therm Eng* 2016;93:920–34.
- [20] Iverson BD, Conboy TM, Pasch JJ, Kruijenga AM. Supercritical CO₂ Brayton cycles for solar-thermal energy. *Appl Energy* 2013;111:957–70.
- [21] Singh R, Kearney MP, Manzie C. Extremum-seeking control of a supercritical carbon-dioxide closed Brayton cycle in a direct-heated solar thermal power plant. *Energy* 2013;60:380–7.
- [22] Zeyghami M, Khalili F. Performance improvement of dry cooled advanced concentrating solar power plants using daytime radiative cooling. *Energy Convers Manage* 2015;106:10–20.
- [23] Padilla RV, Too YCS, Beath A, McNaughton R, Stein W. Effect of pressure drop and reheating on thermal and exergetic performance of supercritical carbon dioxide Brayton cycles integrated with a solar central receiver. *J Sol Energy Eng* 2015;137(5):051012.
- [24] Conboy T, Wright S, Pasch J, Fleming D, Rochau G, Fuller R. Performance characteristics of an operating supercritical CO₂ Brayton cycle. *J Eng Gas Turbines Power* 2012;134(11):111703.
- [25] Luu MT, Milani D, McNaughton R, Abbas A. Advanced control strategies for dynamic operation of a solar-assisted recompression supercritical CO₂ Brayton power cycle. *Appl Therm Eng* 2018;136:682–700.
- [26] Ehsan MM, Wang X, Guan Z, Klimenko A. Design and performance study of dry cooling system for 25 MW solar power plant operated with supercritical CO₂ cycle. *Int J Therm Sci* 2018;132:398–410.
- [27] Ehsan MM, Guan Z, Klimenko A, Wang X. Design and comparison of direct and indirect cooling system for 25 MW solar power plant operated with supercritical CO₂ cycle. *Energy Convers Manage* 2018;168:611–28.
- [28] Ehsan MM, Duniam S, Li J, Guan Z, Gurgenci H, Klimenko A. Effect of cooling system design on the performance of the recompression CO₂ cycle for concentrated solar power application. *Energy* 2019.
- [29] Ehsan MM, Duniam S, Guan Z, Gurgenci H, Klimenko A. Seasonal variation on the performance of the dry cooled supercritical CO₂ recompression cycle. *Energy Convers Manage* 2019;197:111865.
- [30] Neises T, Turchi C. A comparison of supercritical carbon dioxide power cycle configurations with an emphasis on CSP applications. *Energy Procedia* 2014;49:1187–96.
- [31] Turchi CS, Ma Z, Neises TW, Wagner MJ. Thermodynamic study of advanced supercritical carbon dioxide power cycles for concentrating solar power systems. *J Sol Energy Eng* 2013;135(4):041007.
- [32] Wang K, He Y-L, Zhu H-H. Integration between supercritical CO₂ Brayton cycles and molten salt solar power towers: a review and a comprehensive comparison of different cycle layouts. *Appl Energy* 2017;195:819–36.
- [33] Al-Sulaiman FA, Atif M. Performance comparison of different supercritical carbon dioxide Brayton cycles integrated with a solar power tower. *Energy* 2015;82:61–71.
- [34] Kröger DG. Air-cooled heat exchangers and cooling towers. PennWell Books; 2004.
- [35] Dostal V, Hejzlar P, Driscoll MJ. The supercritical carbon dioxide power cycle: comparison to other advanced power cycles. *Nucl Technol* 2006;154(3):283–301.
- [36] S. IPSEpro, "Process Simulation Environment (PSE)," Simtech, Austria; 2003.
- [37] Yoon SH, Kim JH, Hwang YW, Kim MS, Min K, Kim Y. Heat transfer and pressure drop characteristics during the in-tube cooling process of carbon dioxide in the supercritical region. *Int J Refrig* 2003;26(8):857–64.